Am J Physiol Regul Integr Comp Physiol 289: R307–R316, 2005.
First published March 31, 2005; doi:10.1152/ajpregu.00114.2005.

CALL FOR PAPERS | *Metabolic Syndrome*

Reduced nitric oxide bioavailability contributes to skeletal muscle microvessel rarefaction in the metabolic syndrome

Jefferson C. Frisbee

Center for Interdisciplinary Research in Cardiovascular Sciences, Department of Physiology and Pharmacology, West Virginia University, School of Medicine, Morgantown, West Virginia

Submitted 16 February 2005; accepted in final form 29 March 2005

Frisbee, Jefferson C. Reduced nitric oxide bioavailability contributes to skeletal muscle microvessel rarefaction in the metabolic syndrome. *Am J Physiol Regul Integr Comp Physiol* 289: R307–R316, 2005. First published March 31, 2005; doi:10.1152/ajpregu.00114.2005.—This study tested the hypothesis that chronically elevated oxidant stress contributes to impaired active hyperemia in skeletal muscle of obese Zucker rats (OZR) vs. lean Zucker rats (LZR) through progressive deteriorations in microvascular structure. Twelve-week-old LZR and OZR were given 4-hydroxy-2,2,6,6-tetramethylpiperidine 1-oxyl (tempol) in the drinking water for ~4 wk. Subsequently, perfusion of in situ gastrocnemius muscle was determined during incremental elevations in metabolic demand, while a contralateral skeletal muscle arteriole and the gastrocnemius muscle was removed to determine dilator reactivity, vessel wall mechanics, and microvessel density. Under control conditions, active hyperemia was impaired at all levels of metabolic demand in OZR, and this was correlated with a reduced microvessel density, increased arteriolar stiffness, and impaired dilator reactivity. Chronic tempol ingestion improved perfusion during moderate to high metabolic demand only and was associated with improved arteriolar reactivity and microvessel density; passive vessel mechanics were unaltered. Combined antioxidant therapy and nitric oxide synthase inhibition in OZR prevented much of the restored perfusion and microvessel density. In LZR, treatment with N^{ω}-nitro-L-arginine methyl ester (L-NAME) hydrochloride and hydralazine (to prevent hypertension) impaired active hyperemia, dilator reactivity, and microvessel density, although arteriolar distensibility was not altered. These results suggest that with the development of the metabolic syndrome, chronic reductions in nitric oxide bioavailability, in part via the scavenging actions of oxidative free radicals, contribute to a loss of skeletal muscle microvessels, leading to impaired muscle perfusion with elevated metabolic demand.

microcirculation; regulation of skeletal muscle blood flow; functional hyperemia; active hyperemia

A DEVELOPING CHARACTERISTIC of the metabolic syndrome, defined as the combined presentation of obesity, insulin resistance/type II diabetes mellitus, dyslipidemia, and hypertension (1, 2, 48), is a progressive inability to match blood flow to working tissues with metabolic demand arising from those tissues, such that an evolving ischemic condition develops (1). Although this syndrome presently afflicts more than 47 million people in the United States (1, 48), defining specific causes underlying this perfusion/demand mismatch has been challenging, as previous studies in human subjects have determined that alterations to vascular reactivity (12, 13, 15, 31), a progressive structural narrowing of individual vessels (46, 47, 51), and a developing reduction in the density of microvessels within skeletal muscle (38, 58) can all occur during the metabolic syndrome in afflicted individuals. Each of these conditions has the potential to elevate vascular resistance (27, 45) and compromise the ability of skeletal muscle to resist fatigue through impairments in the processes of mass transport and exchange (42, 43, 49, 52).

We have recently investigated skeletal muscle vascular and microvascular consequences of evolution of the metabolic syndrome in the obese Zucker rat (OZR), a model of this condition that results from chronic hyperphagia experienced by the animal as a result of a deficient leptin receptor gene (7, 8). In adult OZR, we have determined that microvessel density within gastrocnemius muscle is markedly reduced and that this reduction contributes, with a structural narrowing of individual skeletal muscle microvessels (18, 54) and an augmentation in vascular α-adrenergic reactivity (17, 55), to elevate the vascular resistance to perfusion and the rate at which skeletal muscle fatigues with elevated metabolic demand (19).

Our previous study examining impairments in skeletal muscle perfusion in OZR has suggested that although an enhanced vascular α-adrenergic reactivity contributes significantly to reduced blood flow under resting conditions, this process does not play a role in blunting muscle perfusion with more substantial increases in metabolic demand (17). We have also previously determined that an acute amelioration of vascular oxidant stress, substantially elevated in OZR, does not improve functional hyperemia in skeletal muscle, despite considerable improvements in the agonist-induced dilator reactivity of arterioles (19, 21, 22). Taken together, these observations suggest that alterations to microvascular structure could play a major role in limiting skeletal muscle perfusion with increased metabolic demand in OZR. Given the observations that the insulin-resistant condition, strongly present in OZR, causes a chronic reduction in the bioavailability of nitric oxide (23, 33, 53) and that previous studies examining mechanisms of angiogenic collateralization have suggested the central importance of nitric oxide bioavailability in the development of new microvessels (25, 35, 40, 41), we hypothesized that chronic reductions in nitric oxide bioavailability, in part via oxidative radical scavenging (4, 58), might contribute to structural alterations to

Address for reprint requests and other correspondence: J. C. Frisbee, Center for Interdisciplinary Research in Cardiovascular Science, Dept. of Physiology and Pharmacology, Robert C. Byrd Health Sciences Center, PO Box 9105, West Virginia Univ. School of Medicine, Morgantown, WV 26505 (E-mail: jfrisbee@hsc.wvu.edu).

The costs of publication of this article were defrayed in part by the payment of page charges. The article must therefore be hereby marked "*advertisement*" in accordance with 18 U.S.C. Section 1734 solely to indicate this fact.

microvascular networks in skeletal muscle of OZR, elevating vascular resistance and impairing functional hyperemic responses.

MATERIALS AND METHODS

Animals. Male lean Zucker rats (LZR) and OZR fed standard chow and tap water ad libitum were used for all experiments. Rats were housed in an American Association for Accreditation of Laboratory Animal Care-accredited animal care facility, and all protocols received prior Institutional Animal Care and Use Committee approval from the Medical College of Wisconsin and West Virginia University. After an overnight fast, rats were anesthetized with injections of pentobarbital sodium (50 mg/kg ip) and received tracheal intubation to facilitate maintenance of a patent airway. In all rats, a carotid artery and an external jugular vein were cannulated for determination of arterial pressure and for both acquisition of blood samples and intravenous infusion of supplemental anesthetic, if necessary. While the rats were under anesthetic, an aliquot of blood was drawn from the jugular vein to be used for the biochemical determination of blood glucose concentration, plasma insulin concentration (Linco), plasma 8-epi-prostaglandin $F_{2\alpha}$ (Cayman), as well as a plasma lipid profile (Sigma) from each animal using commercially available kits.

Preparation of isolated skeletal muscle resistance arterioles. In anesthetized rats, the intramuscular continuation of the right gracilis artery was identified and the vessel was surgically removed. Arterioles were placed in a heated chamber (37°C) that allowed the vessel lumen and exterior to be perfused and superfused, respectively, with physiological salt solution (PSS; equilibrated with 21% O_2, 5% CO_2, 74% N_2) from separate reservoirs. Vessels were cannulated at both ends and were secured to inflow and outflow pipettes connected to a reservoir perfusion system allowing intralumenal pressure and gas concentrations to be controlled. Vessel diameter was measured using television microscopy and an on-screen video micrometer. Arterioles were extended to their in situ length and were equilibrated at 80% of the animal's mean arterial pressure (Table 1).

Subsequent to the initial equilibration period, the reactivity of isolated arterioles was assessed following challenge with: *1)* acetylcholine (10^{-10} M − 10^{-5} M), *2)* hypoxia (ΔPO_2 from ~135 mmHg − ~45 mmHg), and *3)* sodium nitroprusside (10^{-10} M − 10^{-5} M). As the assessment of vascular reactivity was designed to provide an estimation of nitric oxide bioavailability, acetylcholine was used because previous studies have demonstrated that this response in skeletal muscle arterioles is nearly entirely nitric oxide-dependent (22), while responses to hypoxia are partially nitric oxide-dependent (20, 34), and sodium nitroprusside acts as an endothelium-independent nitric oxide donor.

After completion of the above procedures, the perfusate and superfusate were replaced with Ca^{2+}-free PSS, and vessels were treated with 10^{-7} M norepinephrine until reactivity and tone were abolished. At this time, intralumenal pressure within the isolated vessel was altered, in 20-mmHg increments, between 0 mmHg and 160 mmHg, and the inner and outer diameter of the arterioles was determined at each pressure. To ensure that a negative intralumenal pressure was not exerted on the vessel, 5 mmHg was used as the "0 mmHg" intralumenal pressure point; all other values of intralumenal pressure were multiples of 20 mmHg up to 160 mmHg. Specific pressures were randomized to prevent the occurrence of ordering effects. These data were used to calculate arteriolar wall mechanics, which were used as indicators of structural alterations to individual microvessels.

Preparation of in situ blood-perfused skeletal muscle. In LZR and OZR, the left gastrocnemius muscle was isolated in situ, as described previously (19). Briefly, after a medial incision, all muscles, vessels, and connective tissue overlying the gastrocnemius were removed, exposing the gastrocnemius muscle, its vascular supply, and the sciatic nerve. The nerve was double-ligated and sectioned proximally, leaving a ~1-inch length of the nerve to facilitate stimulation of muscle contraction. All branches from the femoral/popliteal artery that did not perfuse the gastrocnemius were ligated or cauterized, depending on size and location. The distal stump of the sciatic nerve was inserted into a stimulating electrode and tied in place. Finally, a microcirculation flow probe (Transonic; 0.5PS or 0.7PS) was placed around the femoral artery, immediately distal to its origin from the iliac artery, to measure gastrocnemius muscle perfusion. The entire preparation was covered in PSS-soaked gauze and plastic film to minimize evaporative water loss and was placed under a lamp to maintain temperature at ~37°C. At this time, heparin (1,500 IU/kg) was infused via the jugular vein to prevent blood coagulation.

Measurement of nitric oxide and superoxide production. From each animal, the right femoral artery was removed, and vascular nitric oxide and superoxide production was assessed using 4,5-diaminofluorescein (DAF-2DA) and dihydroethidine microfluoresence, respectively, as described previously (60). Briefly, DAF-2DA reacts in the presence of NO and O_2 to produce the fluorescent compound triazolofluorescein (DAF-2T) at levels proportional to NO levels (36, 60). Femoral arteries were incubated with DAF-2DA (5×10^{-6} M) for 30 min at 37°C in HEPES buffer. Vessels were rinsed and placed in HEPES buffer with 10^{-4} M L-arginine to maintain substrate bioavailability. The vascular endothelial layer was visualized with a Nikon E 600 microscope (Nikon; Tokyo, Japan) by using an ×10 Plan Fluophase objective. After a 30-min period in which images were acquired every 5 min, images were acquired every 5 min for an additional 30 min after application of the stable acetylcholine analog methacholine (10^{-5} M). Images were acquired using Metamorph Image Acquisition software (Universal Imaging, West Chester, PA) by using a 490-nm wavelength for excitation and a 530-nm wavelength for emission. Acquired images were analyzed for fluorescent intensity, and the rate of nitric oxide generation was calculated as the change in arbitrary units of fluorescent intensity per minute over the respective 30-min period. In a subset of experiments under each condition diethylenetriamine (DETA) NONOate (10^{-4} M) was applied to vessels as a

Table 1. *Baseline characteristics of animals used in the present study*

	Lean Zucker Rats				Obese Zucker Rats		
	Control	Tempol	L-NAME	L-NAME/Hydralazine	Control	Tempol	Tempol/L-NAME
	(n = 8)	(n = 5)	(n = 5)	(n = 5)	(n = 8)	(n = 5)	(n = 5)
Mass, g	351±14	332±18	357±15	350±15	662±17*	660±17*	651±18*
MAP, mmHg	101±5	102±5	126±5*	96±8‡	125±5*	119±5*	137±5*
$[Glucose]_{blood}$, mg/dl	96±12	96±13	99±14	111±16	204±16*	212±16*	218±19*
$[Insulin]_{plasma}$, ng/ml	1.8±0.5	1.5±0.4	1.3±0.5	1.6±0.4	16.2±2.4*	16.1±1.7*	16.8±2.4*
$[Cholesterol]_{plasma}$, mg/dl	59±7	78±10	75±10	81±9	88±9*	140±14*	101±19*
$[Triglycerides]_{plasma}$, mg/dl	69±10	89±18	98±15	102±15	368±20*	368±27*	377±35*
$[8\text{-isoprostane}]_{plasma}$, ng/ml	64±6	48±7	70±8	58±7	139±9*	88±12†	81±9†

Values are presented as means ± SE. *$P < 0.05$ vs. lean Zucker rats (LZR; control); †$P < 0.05$ vs. obese Zucker rats (OZR; control); ‡$P < 0.05$ vs. LZR [N^{ω}-nitro-L-arginine methyl ester (L-NAME)].

positive control and to demonstrate that generation of DAF-2T had not been saturated following challenge with methacholine.

The procedures used to assess vascular superoxide production were similar to those described above for nitric oxide. Briefly, dihydroethidine (DHE) is a lipophilic, cell-permeable dye that is rapidly oxidized into ethidium in the presence of free radical superoxide. The produced ethidium is fixed by intercalation into nuclear DNA, thus giving an indication of oxidant stress within cells under investigation. Segments of the excised femoral arteries were placed in HEPES buffer (37°C) for 30 min. DHE (Molecular Probes) was then added to the vessels for 30 min, and then vessels were rinsed in HEPES buffer. The vascular endothelial layer was visualized using the equipment described above, and images were acquired every 5 min for an hour using a 490-nm wavelength for excitation and a 605-nm wavelength for emission. Acquired images were analyzed for fluorescent intensity, and the rate of superoxide generation was calculated as the change in arbitrary units of intensity per minute over the 60-min period. In select experiments, the mitochondrial superoxide inducer menadione (5×10^{-4} M) and the superoxide dismutate inhibitor sodium diethyldithiocarbamate trihydrate (DETC; 10^{-4} M; Sigma) were added to the vessels simultaneously as a positive control.

Histological determination of microvessel density. At the conclusion of the muscle contraction protocols, the gastrocnemius muscle was removed, rinsed in PSS, and fixed in 0.25% formalin. Muscles were embedded in paraffin and cut into 5-μm cross sections. Sections were incubated with *Griffonia simplicifolia* I lectin (Sigma), as described previously (16, 19, 26). This procedure selectively stains all microvessels with a diameter ≤20 μm, preferentially arterioles and capillaries vs. venules, regardless of perfusion status (26). Sections were rinsed in PSS and were mounted on microscope slides with a water-soluble medium (SP, ACCU-MOUNT 280, Baxter). With the use of fluorescence microscopy, microvessel localization was performed with a Nikon E600 upright microscope with a ×20 objective lens (Plan Fluo phase NA 0.5). Excitation was provided by a 75-Wt Xenon Arc lamp through a Lambda 10–2 optical filter changer (Sutter Instrument, Novato, CA) controlling a 595-nm excitation filter and a 615-nm emission filter. The microscope was coupled to a cooled CCD camera (Micromax; Princeton Instruments, Trenton, NJ). From each gastrocnemius muscle, six individual cross sections were used for analysis, with 6 randomly selected regions within an individual cross section chosen for study. Each region of study had an area of $\sim 1.47 \times 10^5$ μm^2. Within each region studied, all labeled microvessels were counted. All acquired images from individual sections were analyzed for microvessel number using Metamorph imaging software (Universal Imaging, Downingtown, PA).

Experimental protocols. In all protocols, before preparation of the left gastrocnemius muscle, the right gracilis muscle resistance arteriole was surgically removed and isolated for the evaluation of vascular reactivity and passive mechanical characteristics of the vessel wall, described above. Upon completion of the full surgical preparation, the gastrocnemius muscle was stimulated (via the sciatic nerve) to perform bouts of isometric twitch contractions (1, 3, or 5 Hz, 0.4 ms duration, 5V) lasting for 3 min followed by 15 min of self-perfused recovery, with arterial pressure and femoral artery blood flow continuously monitored. After completion of the muscle stimulation protocols, the gastrocnemius muscle was removed, cleared of all nonmuscular tissue and the mass determined. Finally, the muscle was prepared for the determination of microvessel density, and segments of the contralateral femoral artery were removed for assessment of nitric oxide bioavailability and superoxide production, as described above. Initial experiments were performed on LZR ($n = 6$) and OZR ($n = 6$) under control conditions at 16–17 wk of age. To determine the impact of chronic reductions in oxidant stress on the measured parameters, the second series of experiments was performed on 16- to 17-wk-old LZR and OZR that had been given drinking water containing 10^{-3} M 4-hydroxy-2,2,6,6-tetramethylpiperidine 1-oxyl (tempol; Sigma; $n = 5$ for both strains) for the preceding 4–5 wk. For the third series of experiments, 12-wk-old LZR were given drinking water containing either L-NAME ($n = 5$) or L-NAME and hydralazine ($n = 5$) for 4 wk to determine the effects of chronic reductions in nitric oxide bioavailability on perfusion and microvessel structure. The final group (L-NAME + hydralazine) was included to control for the effects of elevated mean arterial pressure which ensues as a result of chronic inhibition of nitric oxide synthase in rats (3, 9). Our previous study demonstrated that treatment with hydralazine had no effect on microvessel density in LZR (16). The final series of experiments determined the effects of a low oxidant stress condition and low nitric oxide bioavailability on microvascular structure/function and skeletal muscle perfusion in OZR. In this protocol, 12-wk-old OZR were given tap water containing L-NAME and tempol ($n = 6$) for 4–5 wk.

Data and Statistical Analyses

Arteriolar reactivity. Dilator responses of isolated arterioles following challenge with acetylcholine or sodium nitroprusside were fit with the three-parameter logistic equation:

$$y = \min + \left[\frac{\max - \min}{1 + 10^{\log ED_{50} - x}} \right]$$

where y represents the change in arteriolar diameter, "min" and "max" represent the lower and upper bounds, respectively, of the change in arteriolar diameter with increasing agonist concentration, x is the logarithm of the agonist concentration and logED_{50} (ED_{50}, half-maximal effective dose) represents the logarithm of the agonist concentration (x) at which the response (y) is halfway between the lower and upper bounds.

Muscle perfusion experiments. Muscle perfusion data were normalized to gastrocnemius muscle mass, which did not differ between LZR (2.4 ± 0.1 g) and OZR (2.3 ± 0.1 g).

Vascular mechanics. The calculations for determining the passive mechanical characteristics of the microvessel wall follow.

Incremental arteriolar distensibility ($DIST_{INC}$; % change in arteriolar diameter/mmHg) was calculated as

$$DIST_{INC} = \frac{\Delta ID}{ID \times \Delta P_{IL}} \times 100$$

where ΔID represents the change in internal arteriolar diameter for each incremental change in intralumenal pressure (ΔP_{IL}).

For the calculation of circumferential stress, intralumenal pressure was converted from mmHg to N/m^2, where 1 mmHg = 1.334×10^2 N/m^2. Circumferential stress (σ) was then calculated as

$$\sigma = \frac{P_{IL} \times ID}{2WT}$$

where WT represents wall thickness (μm; calculated as half of the difference between arteriolar outer diameter and inner diameter). Circumferential strain (ε) was calculated as

$$\varepsilon = \frac{ID - ID_5}{ID_5}$$

where ID_5 represents the internal arteriolar diameter at the lowest intralumenal pressure (i.e., 5 mmHg). Circumferential stress vs. strain curves were fit with an exponential regression equation: $y = \alpha_0 e^{\beta x}$; where y represents circumferential wall stress at a given wall strain x, α_0 represents an intercept term, and β represents a constant related to the rate of increase of the stress vs. strain curve. All fitting of regression equations used ordinary least squares analysis with $r^2 > 0.84$).

All data are presented as means ± SE. For arteriolar reactivity, statistically significant differences in upper bound, logED_{50}, or arteriolar responses to hypoxia were determined using ANOVA. Similarly, differences in individual characteristics describing the extent of

the metabolic syndrome between LZR and OZR, microvessel density within gastrocnemius muscle, the rate of change in fluorescent intensity for nitric oxide or superoxide production, slope coefficients describing the circumferential stress vs. strain relationship, and gastrocnemius muscle perfusion were determined using ANOVA. Differences in arteriolar incremental distensibility between groups were determined using repeated-measures ANOVA. In all cases, a Student-Newman-Keuls post hoc test was used when appropriate and $P < 0.05$ was taken to reflect statistical significance.

RESULTS

Data describing the baseline characteristics of LZR and OZR under the conditions of the present study are summarized in Table 1. At the time of experimentation, OZR were much heavier than LZR and demonstrated a significant elevation in blood pressure, as well as hyperglycemia, hyperinsulinemia, and a severe hypertriglyceridemia. Further, the in vivo marker of lipid peroxidation, 8-epi-prostaglandin $F_{2\alpha}$, was elevated in OZR vs. LZR, indicative of a chronic elevation in oxidant stress within the blood and vascular system. Chronic ingestion of tempol (with or without L-NAME) had no impact on most of the measured characteristics of the metabolic syndrome in OZR but significantly reduced plasma levels of 8-epi-prostaglandin $F_{2\alpha}$, suggesting that this treatment effectively produced a chronic reduction in oxidative stress in OZR. In LZR, chronic blockade of nitric oxide synthase caused a significant increase in mean arterial pressure compared with responses in untreated LZR, although all other measured parameters were unaltered. This hypertensive effect of chronic L-NAME treatment was abolished by concurrent administration of hydralazine.

Data describing the diameter of isolated gracilis muscle resistance arterioles from LZR and OZR under both active and passive conditions in the present study are summarized in Table 2. At the respective equilibration pressures within each experimental group, active arteriolar diameter, although somewhat variable, did not demonstrate statistically significant differences between groups. In contrast, arteriolar diameter under Ca^{2+}-free conditions was significantly reduced in vessels from OZR vs. LZR. As a result of this reduced passive diameter, the active tone in vessels from OZR was also significantly reduced compared with that for vessels from LZR.

The reactivity of skeletal muscle resistance arterioles from LZR and OZR in response to dilator stimuli under the conditions of the present study is summarized in Fig. 1. In untreated OZR, dilator responses to acetylcholine (*A*), hypoxia (*B*), and sodium nitroprusside (*C*) were significantly attenuated compared with levels determined in vessels from untreated LZR.

Table 2. *Resting and passive diameter of isolated arterioles from lean Zucker rats (LZR) and obese Zucker rats (OZR)*

Animal Group	Arteriolar Diameter, μm		Active Tone, %
	Active	Passive	
LZR control	119±3	195±4	39±3
LZR + L-NAME	111±4	184±5	40±4
LZR + L-NAME/hydralazine	116±4	201±4†	42±4
OZR control	113±4	150±5*	25±4*
OZR + Tempol	118±4	153±5*	23±3*
OZR + Tempol/L-NAME	112±5	155±6*	27±4*

Values are presented as means ± SE. All values were determined at the respective equilibration pressure (80% of mean arterial pressure) for the individual animal group. Active tone for vessels was calculated as $(\Delta D/D_{max})\cdot 100$, where ΔD is the diameter increase from rest in response to Ca^{2+}-free PSS and D_{max} is the maximum diameter measured at the equilibration pressure in Ca^{2+}-free PSS. *$P < 0.05$ vs. LZR (control); †$P < 0.05$ vs. LZR (L-NAME).

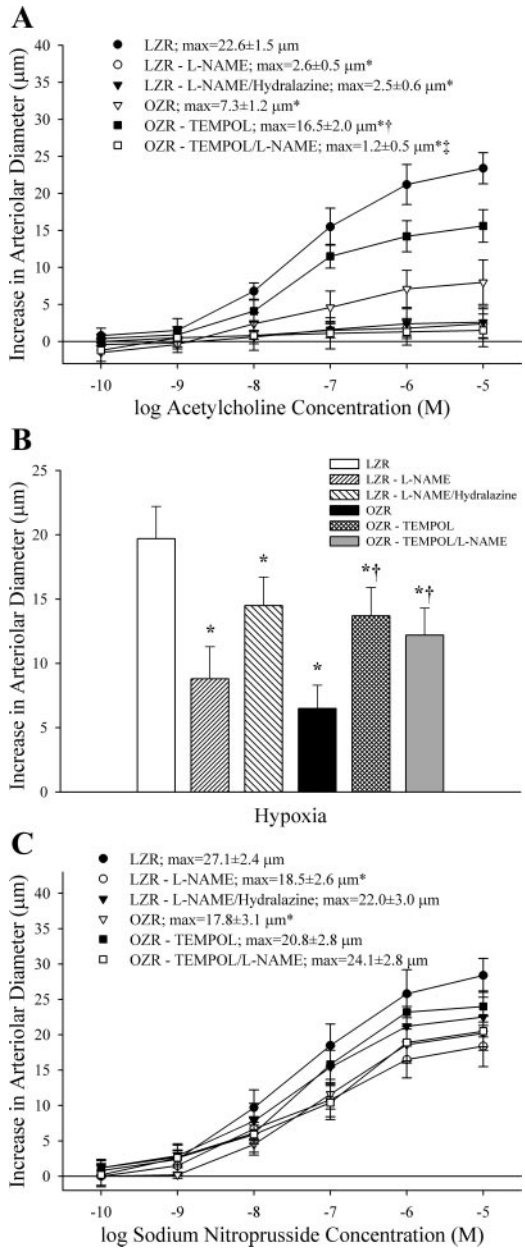

Fig. 1. Data describing the reactivity of skeletal muscle resistance arterioles after challenge with increasing concentrations of acetylcholine (*A*), reduced P_{O_2} (*B*) and increasing concentrations of sodium nitroprusside (*C*). Data (mean ± SE) are presented for arterioles from lean Zucker rats (LZR) and obese Zucker rats (OZR) under control conditions, following chronic NOS inhibition (±hydralazine) in LZR, and following chronic treatment with tempol [±N^{ω}-nitro-L-arginine methyl ester (±L-NAME)] in OZR. For acetylcholine, $logED_{50}$ values were not different between conditions, ranging from −7.6 ± 0.2 M in vessels from OZR (control) to −7.3 ± 0.3 M in vessels from OZR + tempol. Similarly, for sodium nitroprusside, $logED_{50}$ values were not different between conditions, ranging from −7.5 ± 0.2 M in vessels from LZR (control) to −7.2 ± 0.2 M in vessels from OZR (control). *$P < 0.05$ vs. response in arterioles from untreated LZR, †$P < 0.05$ vs. responses in arterioles from untreated OZR, ‡$P < 0.05$ vs. responses in arterioles from OZR chronically treated with tempol.

Chronic treatment with tempol alone, while having no significant effect on dilator responses in vessels of LZR (data not shown), significantly enhanced both acetylcholine-induced and hypoxic dilation in vessels from OZR, although responses remained blunted compared with those in untreated LZR. In response to chronic nitric oxide synthase (NOS) inhibition, the reactivity of arterioles from LZR in response to acetylcholine or reduced P_{O_2} was severely attenuated, while sodium nitroprusside-induced dilation was largely unaltered. In animals receiving combined NOS blockade and antihypertensive therapy, the abrogated acetylcholine-induced dilation determined in response to L-NAME treatment alone was not altered, although the dilator response to hypoxia was improved. Combined chronic treatment with tempol and L-NAME severely attenuated dilator responses to acetylcholine in OZR, although responses to hypoxia were only mildly blunted compared with tempol treatment alone, and responses to sodium nitroprusside were largely unaffected.

The results of the fluorescence microscopy evaluation of vascular nitric oxide bioavailability and superoxide production are presented in Fig. 2. In untreated OZR, both basal (*A*) and methacholine-stimulated (*B*) production of nitric oxide was blunted vs. levels determined in vessels from untreated LZR. Chronic tempol treatment increased both basal and stimulated nitric oxide bioavailability in OZR, although these values were still reduced vs. those determined in vessels from LZR. The presence of chronic L-NAME treatment, in either strain, under any condition, severely abrogated nitric oxide bioavailability under both basal and methacholine-stimulated conditions. Application of DETA NONOate resulted in a substantial increase in fluorescent intensity in vessels from both strains under all conditions (data not shown).

OZR exhibited a substantial increase in the rate of vascular superoxide production compared with responses determined in LZR (Fig. 2*C*). In contrast, superoxide generation was attenuated in vessels from OZR in response to chronic treatment with tempol compared with responses in vessels from untreated animals. Baseline vascular superoxide generation was not significantly altered in response to chronic treatment with L-NAME in LZR. In OZR, combined chronic treatment with both tempol and L-NAME had minimal impact on vascular superoxide production compared with responses determined following chronic tempol treatment alone. Acute treatment of vessels of LZR and OZR with tempol abolished differences in oxidant stress between the strains, while treatment with menadione and DETC caused a significant increase in the rate of superoxide generation in vessels from both LZR and OZR (data not shown).

Figure 3 presents data describing the mechanics of the skeletal muscle resistance arteriolar wall in OZR and LZR. Under Ca^{2+}-free conditions, arteriolar incremental distensibility was reduced in OZR compared with LZR (*A*), and there was a left shift in the circumferential wall stress vs. strain relationship (*B*). Chronic treatment of OZR with the superoxide dismutase mimetic alone did not alter the mechanics of the arteriolar wall compared with responses determined in vessels from untreated OZR. Tempol treatment also had no impact on these responses in vessels from LZR (data not shown). Chronic NOS inhibition alone caused a consistent, although not statistically significant ($P = 0.141$), decrease in arterial distensibility and a left shift in the stress vs. strain relationship in

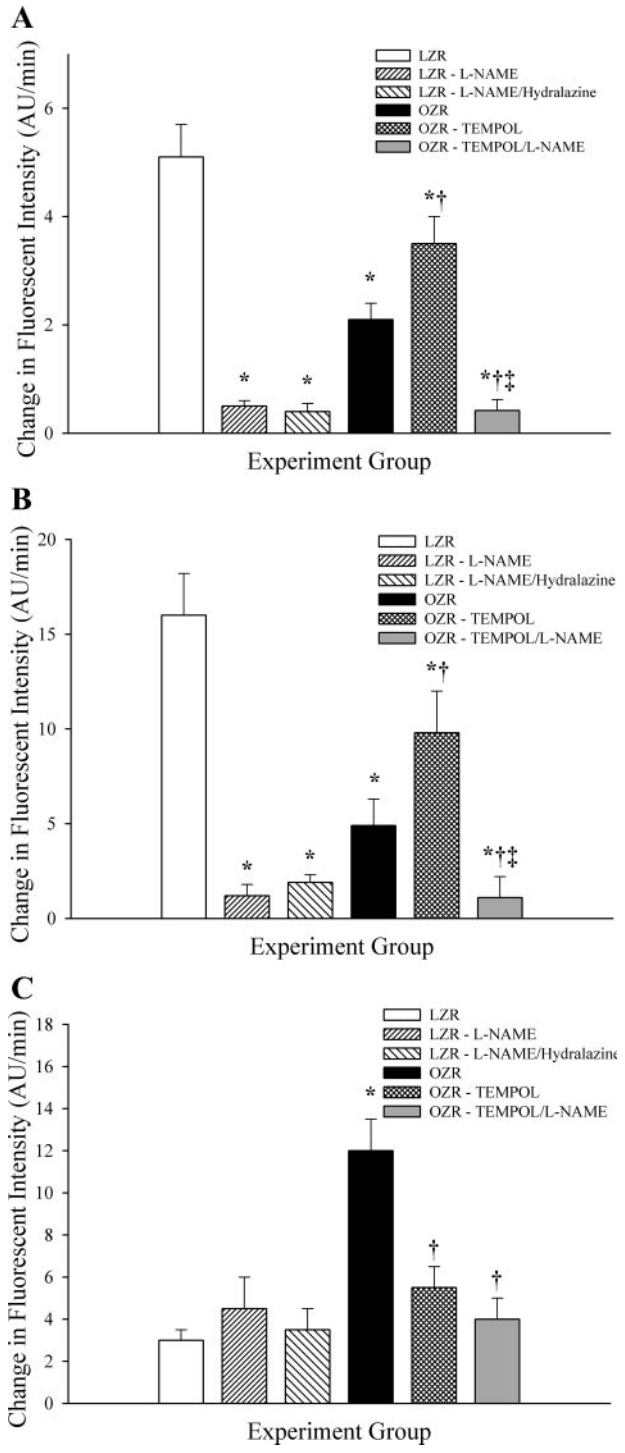

Fig. 2. The rate of vascular nitric oxide production under basal (*A*) and methacholine-stimulated (*B*) conditions and the rate of superoxide generation (*C*) in femoral arteries from LZR and OZR, as determined using diaminofluorescein and dihydroethidine fluorescence microscopy, respectively. Data (mean ± SE) describe the rate of change in nitric oxide or superoxide production as the increase in arbitrary units of fluorescent intensity per minute. Data are presented for arteries from LZR and OZR under control conditions, following chronic NOS inhibition (±hydralazine) in LZR, and following chronic treatment with tempol (±L-NAME) in OZR. *$P < 0.05$ vs. response in untreated LZR, †$P < 0.05$ vs. response in untreated OZR, ‡$P < 0.05$ vs. response from OZR chronically treated with tempol.

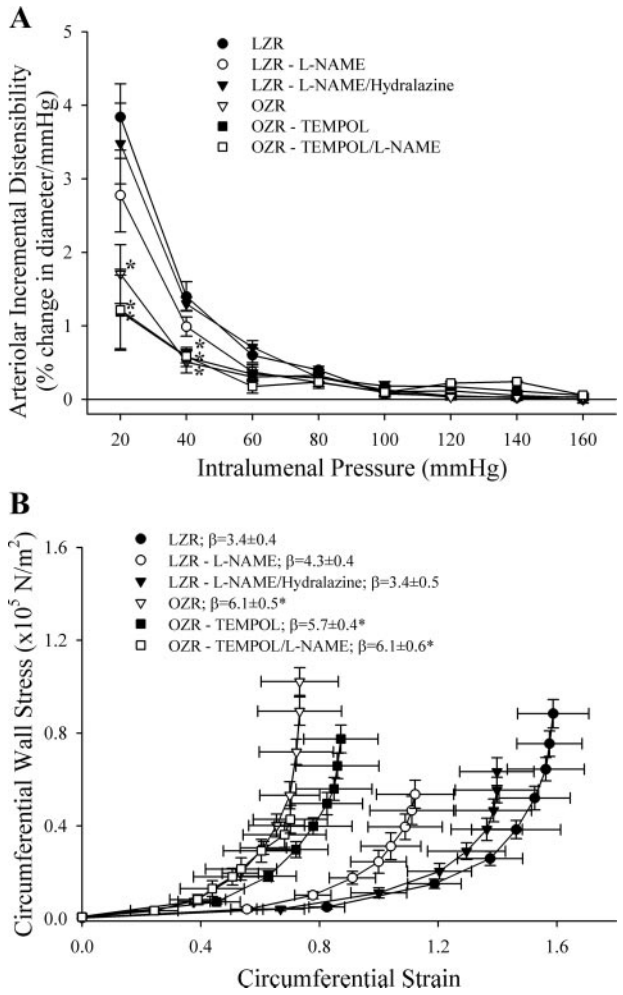

Fig. 3. Data describing the mechanics of the wall of isolated gracilis muscle resistance arterioles from LZR and OZR under passive (Ca^{2+}-free) conditions. *A*: calculated incremental distensibility of the arteriolar wall from LZR and OZR with elevated intralumenal pressure. *B*: circumferential wall stress vs. strain relation for vessels of lean and obese Zucker rats. Data (mean ± SEM) are presented for arterioles from LZR and OZR under control conditions, following chronic NOS inhibition (±hydralazine) in LZR, and after chronic treatment with tempol (±L-NAME) in OZR. *$P < 0.05$ vs. response in arterioles from untreated LZR.

arterioles of LZR. Combined treatment with hydralazine completely abolished any increase in vascular stiffness in LZR. In OZR, chronic concurrent ingestion of tempol and L-NAME had no effect on incremental distensibility and the stress vs. strain relation compared with vessels of OZR treated with tempol only.

Figure 4 presents gastrocnemius muscle microvessel density in LZR and OZR. As shown in Fig. 4, microvessel density in untreated OZR was significantly reduced compared with levels in untreated LZR. While chronic treatment with tempol alone had no impact on microvessel density in gastrocnemius muscle of LZR (data not shown), tempol treatment reduced the extent of the microvascular rarefaction in skeletal muscle of OZR. In LZR, chronic NOS inhibition resulted in a decreased gastrocnemius muscle microvessel density compared with that in untreated LZR. However, combined treatment of L-NAME and hydralazine (to eliminate any confounding influence of elevated mean arterial pressure) did not significantly improve microvessel density from levels determined in LZR treated with L-NAME alone. In OZR, combined treatment with tempol and L-NAME prevented any recovery in microvessel density brought about by chronic ingestions of the oxidative radical scavenger alone.

Data describing skeletal muscle perfusion in OZR and LZR under resting conditions and with increased metabolic demand are presented in Fig. 5. Gastrocnemius muscle blood flow was significantly reduced in untreated OZR compared with levels determined in control LZR under resting conditions, and in response to 3 min of muscle contraction at 1, 3, or 5 Hz isometric twitch contractions. Chronic ingestion of tempol did not alter skeletal muscle perfusion in OZR under resting conditions, or in response to a 1-Hz twitch contraction. In contrast, during 3 Hz, and more so during 5 Hz twitch contraction, chronic treatment of OZR with the superoxide dismutase mimetic resulted in an increased skeletal muscle perfusion compared with levels determined in untreated OZR. The hyperemic responses of the contracting gastrocnemius of LZR were not altered by the imposed tempol regimen (data not shown). With chronic L-NAME treatment, gastrocnemius muscle blood flow in LZR was comparable to that in untreated LZR both at rest and in response to a 1-Hz twitch contraction. However, with increased metabolic demand, LZR that received NOS inhibition exhibited an increased degree of ischemia compared with responses in control rats. With 3-Hz twitch contraction, perfusion was attenuated in LZR receiving NOS inhibition, although this did not reach statistical significance ($P = 0.101$). Combined treatment of L-NAME and hydralazine did not alter these relationships. In OZR, combined treatment with tempol and L-NAME abolished the improved active hyperemic response determined following chronic tempol treatment alone, such that both resting blood flow and all active hyperemic responses were not significantly different from that determined in OZR under untreated conditions.

DISCUSSION

Our previous studies have demonstrated that the reactivity of skeletal muscle resistance arterioles is dramatically altered with development of the metabolic syndrome in the Zucker rat,

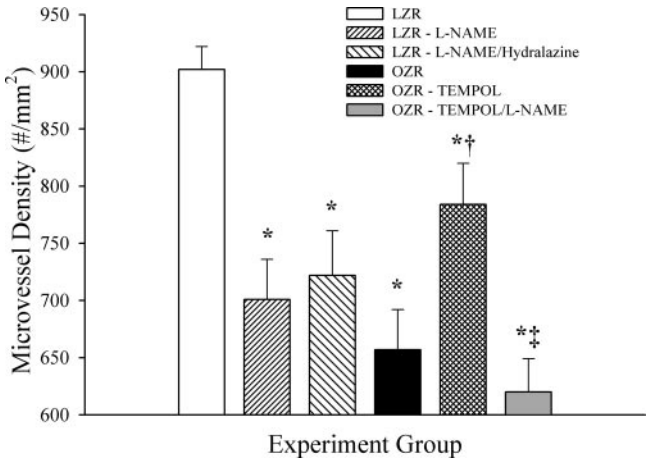

Fig. 4. Data (mean ± SEM) describing gastrocnemius muscle microvessel density (*A*) in LZR and OZR at 16–17 wk of age under the conditions of the present study. *$P < 0.05$ vs. untreated LZR; †$P < 0.05$ vs. untreated OZR; ‡$P < 0.05$ vs. OZR treated with tempol.

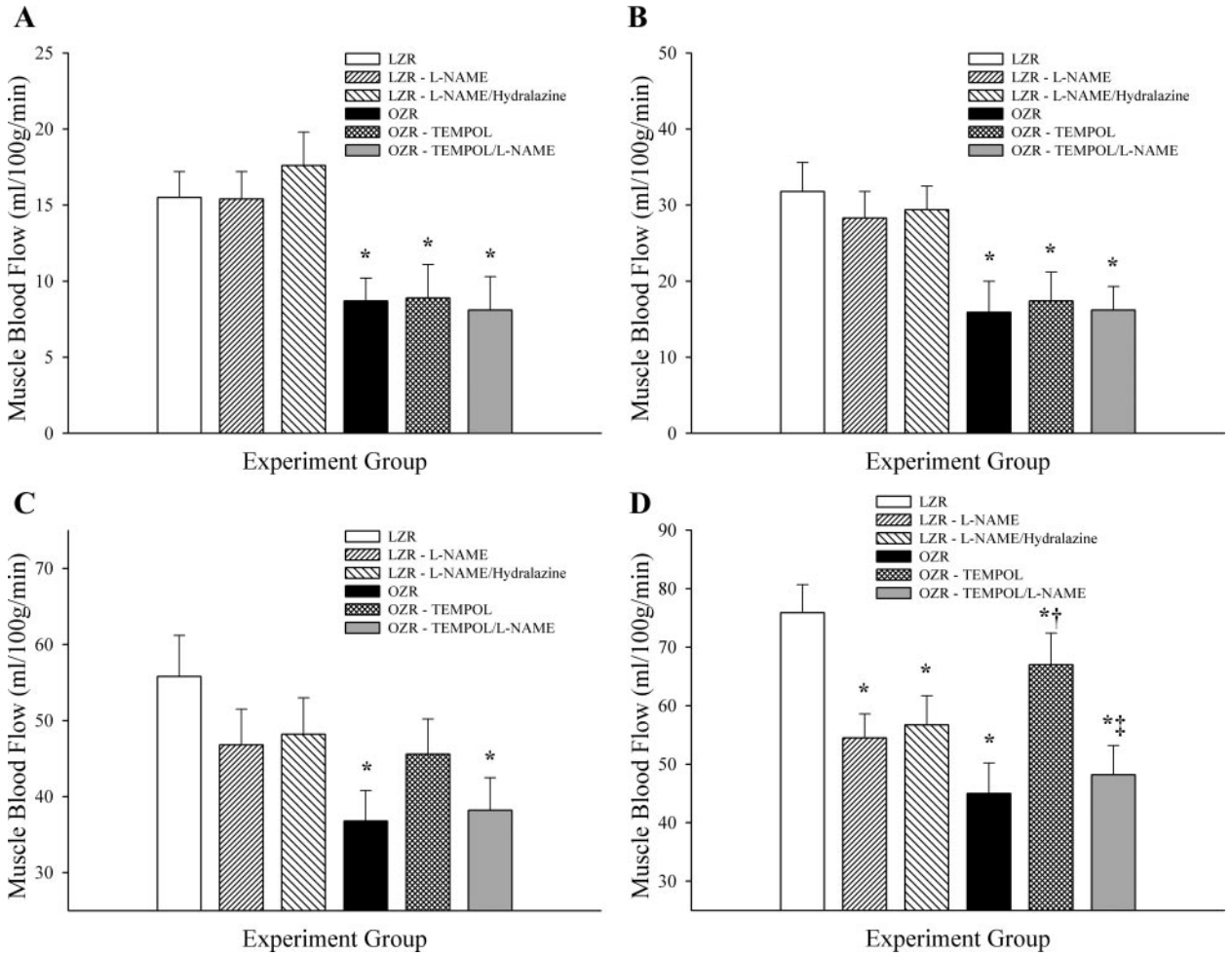

Fig. 5. Gastrocnemius muscle blood flow in LZR and OZR under resting conditions (*A*) and in response to 3 min of elevated metabolic demand, imposed via 1 Hz (*B*), 3 Hz (*C*) and 5 Hz (*D*) isometric twitch contractions. Data (mean ± SE) are presented for arterioles from LZR and OZR under control conditions, after chronic NOS inhibition (±hydralazine) in LZR, and after chronic treatment with tempol (±L-NAME) in OZR. *$P < 0.05$ vs. untreated LZR, †$P < 0.05$ vs. untreated OZR, ‡$P < 0.05$ vs. OZR treated with tempol.

characterized by profound impairments to dilator reactivity and enhanced constrictor responses to both myogenic and α-adrenergic activation (19). Although the impaired dilation and enhanced myogenic activity were partly a function of elevated vascular oxidant tone, the augmented α-adrenergic constriction was independent of oxidative stress and reflected alterations that were intrinsic to that signaling mechanism. In addition, structural modifications to individual microvessels were reflected in a reduced vessel wall distensibility (18, 54), while vascular networks were modified through ongoing reductions in microvessel density (16, 18). These influences combined to create an underperfusion of in situ skeletal muscle in OZR, both at rest and in response to elevated metabolic demand (17, 19). However, attempts to improve perfusion through acute reduction in oxidant stress were unsuccessful. Whereas several indices of vascular reactivity were improved, basal blood flow to, and active hyperemic responses of, skeletal muscle were unaltered (19). These observations, combined with our study demonstrating that the increased α-adrenergic reactivity of skeletal muscle arterioles restrains perfusion at rest and with mild-moderate elevations in metabolic demand only (17), suggested that alterations to vascular structure may contribute to skeletal muscle underperfusion in OZR during more profound increases in metabolic intensity.

The present results derived from LZR and OZR under control conditions provide support for our conceptual model. By 17 wk of age, OZR demonstrated all of the systemic markers for the metabolic syndrome, as defined in this study (Table 1). Specifically, OZR were obese, markedly insulin resistant, dyslipidemic, with a moderate hypertension and an elevated in vivo oxidant stress [estimated using plasma levels of 8-epi-prostaglandin $F_{2\alpha}$ (29)]. Skeletal muscle arteriolar reactivity to endothelium-dependent stimuli was strongly impaired in OZR (Fig. 1), and this was associated with systemic vascular environment characterized by high oxidant stress and low nitric oxide bioavailability (Fig. 2). Structurally, individual resistance arterioles were less distensible in OZR (Fig. 3), and skeletal muscle microvascular networks were strongly rarefied (Fig. 4). As a result, both basal perfusion and active hyperemia were blunted in muscle of OZR vs. LZR (Fig. 5).

Given that a predominant effect of elevated superoxide production is nitric oxide scavenging (4, 58), we attempted to ameliorate this process through chronic treatment of OZR with tempol. The underlying premise of this protocol was that, if

altered microvascular structure were a stronger contributor to underperfusion of skeletal muscle during elevated metabolic demand than was impaired vascular reactivity, acute antioxidant therapy could not be expected to have a restorative influence on hyperemic responses (19). Chronic tempol treatment in OZR reduced plasma levels of 8-epi-prostaglandin $F_{2\alpha}$, although other systemic indices of the metabolic syndrome were unaffected (Table 1). Additionally, the effectiveness of chronic tempol treatment in reducing the oxidative environment was also evidenced in a reduced vascular superoxide production and increased nitric oxide bioavailability in OZR (Fig. 2). This lowered oxidant stress was associated with an improved arteriolar reactivity to stimuli that were both predominantly (acetylcholine) and partially (hypoxia) dependent on the nitric oxide bioavailability (Fig. 1). Interestingly, structural alterations to the microcirculation under this condition were limited to an improved skeletal muscle microvessel density alone (Fig. 4), as chronic treatment with the antioxidant had no effect on arteriolar wall mechanics (Fig. 3). The combined effect of these results was that active hyperemia in skeletal muscle of OZR was improved at moderate-high metabolic demand (Fig. 5). The absence of improvement in skeletal muscle perfusion at rest and during lower levels of metabolic demand may not have been surprising for two reasons. First, it is less likely that structural constraints on perfusion would exert themselves and be discernible at lower levels of blood flow (18, 45). Second, our recent study suggests that the enhanced α-adrenergic tone of skeletal muscle arterioles is a stronger influence reducing blood flow in OZR under resting conditions and with lower elevations in metabolic demand than other structural or functional variables (17). These results clearly suggest that creation of chronic condition of more normal oxidant stress with improved nitric oxide bioavailability in OZR can contribute to a restoration of skeletal muscle perfusion with elevated metabolic demand. However, while our recent work strongly suggests that this improved perfusion in skeletal muscle of OZR is a function of a more normal vascular network structure (19), we cannot confidently rule out a contributing role for an enhanced reactivity of skeletal muscle microvessel at this time.

Given these results, and the recent work of others examining the effects of chronic reductions in nitric oxide bioavailability on microvascular network structure (25, 35, 40, 41), LZR were treated with L-NAME to investigate the effects of low nitric oxide bioavailability per se without the confounding influence of elevated oxidant stress on microvascular structure and function and skeletal muscle perfusion. Chronic inhibition of nitric oxide synthase did not impact any of the systemic measurements in LZR, with the singular exception of mean arterial pressure (abolished by concurrent treatment with hydralazine). The effectiveness of chronic NOS inhibition in attenuating nitric oxide bioavailability was clear, as arteriolar dilation in response to acetylcholine was completely abolished (Fig. 1) and both basal and methacholine-stimulated nitric oxide production were blunted, with minimal changes in vascular superoxide production (Fig. 2). Chronic NOS inhibition caused a mild increase in the stiffness of individual vessels, which was attributable to the elevated mean arterial pressure, as combined treatment with hydralazine completely prevented this. In contrast, chronic NOS inhibition reduced microvessel density in LZR, and this effect was independent of arterial pressure, as concurrent treatment with hydralazine did not restore vascularity. From a functional perspective, this chronic reduction in nitric oxide bioavailability resulted in a blunted active hyperemia at higher metabolic intensities, although perfusion at rest and with mild elevations in metabolic demand was unaltered. These results suggest that the chronic reduction in nitric oxide bioavailability may have been a significant stimulus for microvascular rarefaction in LZR.

Applying these results to OZR, it was reasonable to hypothesize that chronically low nitric oxide bioavailability may be the stimulus for microvascular rarefaction and that elevated oxidant tone may represent a mechanism for reducing bioavailability rather than prima facie cause of the rarefaction itself. The final set of experiments, which combined treatment of OZR with tempol (±L-NAME) allowed for comparisons of skeletal muscle microvascular function and perfusion under control conditions, under conditions of low oxidant stress/elevated nitric oxide bioavailability (tempol), and under conditions of low oxidant stress/low nitric oxide bioavailability (tempol + L-NAME). The results from these experiments demonstrated that chronic ingestion of tempol + L-NAME created a condition of low oxidant tone and low nitric oxide bioavailability, compared with that for tempol treatment alone or under control conditions in OZR (Table 1, Figs. 1 and 2). Although the structure of individual microvessels does not appear to be influenced by oxidant status in OZR (Fig. 3), the reduced microvessel density in OZR under control conditions, improved in low oxidant stress/high nitric oxide bioavailability conditions following tempol treatment, was reduced toward control levels by the combined treatment with tempol and L-NAME (Fig. 4). Thus, despite lowering of oxidant stress following tempol treatment, any improvement in microvessel density was only observed under conditions where nitric oxide bioavailability was also improved. Finally, the reductions in nitric oxide bioavailability reduced the improved active hyperemia in OZR from those identified in OZR treated with tempol back to levels that were not different from those in control OZR.

Taken together, these results suggest that skeletal muscle microvessel density in the Zucker rat model of the metabolic syndrome may be more closely a function of chronic nitric oxide bioavailability rather than chronic oxidant stress. Although oxidant stress certainly appears to act as a contributor to the reductions in nitric oxide bioavailability, other processes impacting bioavailability may also contribute to this net reduction. With specific relevance for the development of the metabolic syndrome, work from Bohlen's laboratory has demonstrated that increased activity and expression of protein kinase C constrains nitric oxide bioavailability in mesenteric microvessels of the Zucker diabetic fatty (ZDF) rat (5, 6), such that dilation to elevated flow rate and reduced P_{O_2} are impaired. Further, recent study has shown that the availability of tetrahydrobiopterin (BH_4), a necessary cofactor for nitric oxide production, is diminished in ZDF rats (11, 44). Additional influences on nitric oxide bioavailability may include a limitation on the availability of L-arginine as a substrate (28) and the effects of the endogenous inhibitor of nitric oxide synthase, asymmetric dimethylarginine (ADMA), the concentration of which has recently been shown to be elevated in individuals afflicted with multiple components of the metabolic syndrome (10, 14, 37, 38, 56, 57). When integrated with studies suggest-

ing that endothelial NOS expression is not reduced in OZR vs. LZR (23, 32, 50), further investigation into how these myriad processes contribute to the chronic reductions in nitric oxide bioavailability and how these may interact with the chronic elevations in oxidant stress represents an avenue for ongoing investigation.

Of most direct relevance to the present study may be recent work from Gealekman et al. (24). In that study, microvascular density within the kidney of 8- and 22-wk-old ZDF rats was determined following chronic treatment with a peroxynitrite scavenger to assess the effects of oxidant scavenging of nitric oxide and the resulting generation of peroxynitrite on angiogenic responses. In that study, the authors determined that renal capillary density in ZDF rats was decreased at 22 wk and that the angiogenic competence of renal explants was impaired. However, treatment with scavenging of peroxynitrite partially prevented the decreased renal capillary density and explant angiogenic competence in ZDF rats. The results of both the present experiments and this recent study are compatible, in that both suggest that a balance between oxidant production, nitric oxide bioavailability, and the production of endproducts (i.e., peroxynitrite) may exist in the metabolic syndrome, wherein the balance between microvessel generation and regression is offset, producing a net rarefaction within diverse tissues. It should be emphasized that tempol, a cell-permeable superoxide dismutase mimetic, facilitates the dismutation reaction of superoxide and slows the scavenging of nitric oxide and the resulting production of peroxynitrite. As such, when incorporated with a previous study (24), the present results do not rule out the possibility that the beneficial effects of chronic tempol treatment may also occur via a nonspecific downstream effect of the increased nitric oxide bioavailability (e.g., reduced peroxynitrite formation).

ACKNOWLEDGMENTS

The author expresses his thanks to Dr. Jiaxhuan Zhu, Glenn Slocum, Camille Torres, Lisa Henderson, Anne Ansley and Brian Corson at the Department of Physiology at the Medical College of Wisconsin for their expert technical assistance during the performance of specific elements of the present study.

GRANTS

This work was funded by the American Heart Association (0330194N) and the National Institutes of Health (R01-DK64668).

REFERENCES

1. **American Diabetes Association.** Statistical Summary Pages. http://www.diabetes.org/diabetes-statistics.jsp, 2004.
2. **American Heart Association.** Statistical Summary Pages. www.americanheart.org/presenter.jhtml?identifier=2016, 2004.
3. **Bauersachs J, Bouloumie A, Fraccarollo D, Hu K, Busse R, and Ertl G.** Hydralazine prevents endothelial dysfunction, but not the increase in superoxide production in nitric oxide-deficient hypertension. *Eur J Pharmacol* 362:77–81, 1998.
4. **Beckman JS and Koppenol WH.** Nitric oxide, superoxide, and peroxynitrite: the good, the bad, and ugly. *Am J Physiol Cell Physiol* 271: C1424–C1437, 1996.
5. **Bohlen HG.** Protein kinase βII in Zucker obese rats compromises oxygen and flow-mediated regulation of nitric oxide formation. *Am J Physiol Heart Circ Physiol* 286: H492–H497, 2004.
6. **Bohlen HG and Nase GP.** Obesity lowers hyperglycemic threshold for impaired in vivo endothelial nitric oxide function. *Am J Physiol Heart Circ Physiol* 283: H391–H397, 2002.
7. **Bray GA.** The Zucker-fatty rat: a review. *Fed Proc* 36:148–153, 1977.
8. **Bray GA and York DA.** Genetically transmitted obesity in rodents. *Physiol Rev* 51: 598–646, 1971.
9. **Casellas D, Benahmed S, Artuso A, and Jover B.** Candesartan and progression of preglomerular lesions in N(G)-nitro-L-arginine methyl ester hypertensive rats. *J Am Soc Nephrol* 10: S230–S233, 1999.
10. **Chan NN and Chan JC.** Asymmetric dimethylarginine (ADMA): a potential link between endothelial dysfunction and cardiovascular diseases in insulin resistance syndrome? *Diabetologia* 45:1609–1616, 2002.
11. **Chander PN, Gealekman O, Brodsky SV, Elitok S, Tojo A, Crabtree M, Gross SS, and Goligorsky MS.** Nephropathy in Zucker diabetic fat rat is associated with oxidative and nitrosative stress: prevention by chronic therapy with a peroxynitrite scavenger ebselen. *J Am Soc Nephrol* 15: 2391–2403, 2004.
12. **de Jongh RT, Serne EH, Ijzerman, RG, de Vries, G, and Stehouwer CDA.** Impaired microvascular function in obesity: implications for obesity-associated microangiopathy, hypertension, and insulin resistance. *Circulation* 109: 2529–2535, 2004.
13. **Dell'Omo G, Penno G, Pucci L, Mariani M, Del Prato S, and Pedrinelli R.** Abnormal capillary permeability and endothelial dysfunction in hypertension with comorbid metabolic syndrome. *Atherosclerosis* 172: 383–389, 2004.
14. **Eid HM, Arnesen H, Hjerkinn EM, Lyberg T, and Seljeflot I.** Relationship between obesity, smoking, and the endogenous nitric oxide synthase inhibitor, asymmetric dimethylarginine. *Metabolism* 53: 1574–1579, 2004.
15. **Esler M, Rumantir M, Wiesner G, Kaye D, Hastings J, and Lambert G.** Sympathetic nervous system and insulin resistance: from obesity to diabetes. *Am J Hypertens* 14:304S-309S, 2001.
16. **Frisbee JC.** Hypertension-independent microvascular rarefaction in the obese Zucker rat model of the metabolic syndrome. *Microcirculation* In press.
17. **Frisbee JC.** Enhanced arteriolar alpha-adrenergic constriction impairs dilator responses and skeletal muscle perfusion in obese Zucker rats. *J Appl Physiol* 97:764–772, 2004.
18. **Frisbee JC.** Remodeling of the skeletal muscle microcirculation increases resistance to perfusion in obese Zucker rats. *Am J Physiol Heart Circ Physiol* 285: H104–H111, 2003.
19. **Frisbee JC.** Impaired skeletal muscle perfusion in obese Zucker rats. *Am J Physiol Regul Integr Comp Physiol* 285: R1124–R1134, 2003.
20. **Frisbee JC, Maier KG, Falck JR, Roman RJ, and Lombard JH.** Integration of hypoxic dilation signaling pathways for skeletal muscle resistance arteries. *Am J Physiol Regul Integr Comp Physiol* 283: R309–R319, 2002.
21. **Frisbee JC.** Impaired dilation of skeletal muscle resistance arteries to reduced oxygen tension in the diabetic obese Zucker rat. *Am J Physiol Heart Circ Physiol* 281: H1568–H1574, 2001.
22. **Frisbee JC and Stepp DW.** Impaired nitric oxide-dependent dilation of skeletal muscle arterioles in diabetic obese Zucker rats. *Am J Physiol Heart Circ Physiol* 281: H1304–H1311, 2001.
23. **Fulton D, Harris MB, Kemp BE, Venema RC, Marrero MB, and Stepp DW.** Insulin resistance does not diminish eNOS expression, phosphorylation, or binding to HSP-90. *Am J Physiol Heart Circ Physiol* 287: H2384–H2393, 2004.
24. **Gealekman Brodsky OSV, Zhang F, Chandler PN, Friedli C, Nasjletti A, and Goligorsky MS.** Endothelial dysfunction as a modifier of angiogenic response in Zucker diabetic fat rat: amelioration with Ebselen. *Kidney Int* 66: 2337–2347, 2004.
25. **Girardot D, Jover B, Moles JP, Deblois D, and Moreau P.** Chronic nitric oxide synthase inhibition prevents new coronary capillary generation. *J Cardiovasc Pharmacol* 44: 322–328, 2004.
26. **Greene AS, Lombard JH, Cowley AW Jr, and Hansen-Smith FM.** Microvessel changes in hypertension measured by *Griffonia simplicifolia* I lectin. *Hypertension* 15:779–783, 1990.
27. **Greene AS, Tonellato PJ, Lui J, Lombard JH, and Cowley AW Jr.** Microvascular rarefaction and tissue vascular resistance in hypertension. *Am J Physiol Heart Circ Physiol* 256: H126–H131, 1989.
28. **Gur S, Ozturk B, and Karahan ST.** Impaired endothelium-dependent and neurogenic relaxation of corpus cavernosum from diabetic rats: improvement with L-arginine. *Urol Res* 28:14–19, 2000.
29. **Hansel B, Giral P, Nobecourt E, Chantepie S, Bruckert E, Chapman MJ, and Kontush A.** Metabolic syndrome is associated with elevated oxidative stress and dysfunctional dense high-density lipoprotein particles displaying impaired antioxidative activity. *J Clin Endocrinol Metab* 89: 4963–4971, 2004.

30. **Hoagland KM, Maier KG, Roman RJ.** Contributions of 20-HETE to the antihypertensive effects of Tempol in Dahl salt-sensitive rats. *Hypertension* 41:697–702, 2003.
31. **Hsueh WA and Quinones MJ.** Role of endothelial dysfunction in insulin resistance. *Am J Cardiol* 92:10J-17J, 2003.
32. **Karagiannis J, Reid JJ, Darby I, Roche P, Rand MJ, and Li CG.** Impaired nitric oxide function in the basilar artery of the obese Zucker rat. *J Cardiovasc Pharmacol* 42: 497–505, 2003.
33. **Katakam PV, Tulbert CD, Snipes JA, Erdos B, Miller AW, and Busija DW.** Impaired insulin-induced vasodilation in small coronary arteries of Zucker obese rats is mediated by reactive oxygen species. *Am J Physiol Heart Circ Physiol* 288: H854–H860, 2005.
34. **Kerkhof CJ, Bakker EN, and Sipkema P.** Role of cytochrome P-450 4A in oxygen sensing and NO production in rat cremaster resistance arteries. *Am J Physiol Heart Circ Physiol* 277: H1546–H1552, 1999.
35. **Kiefer FN, Misteli H, Kalak N, Tschudin K, Fingerle J, Van der Kooij M, Stumm M, Sumanovski LT, Sieber CC, and Battegay EJ.** Inhibition of NO biosynthesis, but not elevated blood pressure, reduces angiogenesis in rat models of secondary hypertension. *Blood Press* 11: 116–124, 2002.
36. **Kojima H, Nakatsubo N, Kikuchi K, Kawahara S, Kirino Y, Nagoshi H, Hirata Y, and Nagano T.** Detection and imaging of nitric oxide with novel fluorescent indicators: diaminofluoresceins. *Anal Chem* 70: 2446–2453, 1998.
37. **Krzyzanowska K, Mittermayer F, Kopp HP, Wolzt M, and Schernthaner G.** Weight loss reduces circulating asymmetrical dimethylarginine concentrations in morbidly obese women. *J Clin Endocrinol Metab* 89:6277–6281, 2004.
38. **Lin KY, Ito A, Asagami T, Tsao PS, Adimoolam S, Kimoto M, Tsuji H, Reaven GM, and Cooke JP.** Impaired nitric oxide synthase pathway in diabetes mellitus: role of asymmetric dimethylarginine and dimethylarginine dimethylaminohydrolase. *Circulation* 106: 987–992, 2002.
39. **Lind L and Lithell H.** Decreased peripheral blood flow in the pathogenesis of the metabolic syndrome comprising hypertension, hyperlipidemia, and hyperinsulinemia. *Am Heart J* 125:1494–1497, 1993.
40. **Lloyd PG, Yang HT, and Terjung RL.** Arteriogenesis and angiogenesis in rat ischemic hindlimb: role of nitric oxide. *Am J Physiol Heart Circ Physiol* 281: H2528–H2538, 2001.
41. **Matsunaga T, Warltier DC, Weihrauch DW, Moniz M, Tessmer J, and Chilian WM.** Ischemia-induced coronary collateral growth is dependent on vascular endothelial growth factor and nitric oxide. *Circulation* 102: 3098–3103, 2000.
42. **McGuire BJ and Secomb TW.** Estimation of capillary density in human skeletal muscle based on maximal oxygen consumption rates. *Am J Physiol Heart Circ Physiol* 285: H2382–H2391, 2003.
43. **McGuire BJ and Secomb TW.** A theoretical model for oxygen transport in skeletal muscle under conditions of high oxygen demand. *J Appl Physiol* 91: 2255–2265, 2001.
44. **Meininger CJ, Cai S, Parker JL, Channon KM, Kelly KA, Becker EJ, Wood MK, Wade LA, and Wu G.** GTP cyclohydrolase I gene transfer reverses tetrahydrobiopterin deficiency and increases nitric oxide synthesis in endothelial cells and isolated vessels from diabetic rats. *FASEB J* 18:1900–1902, 2004.
45. **Milnor WR.** Hemodynamics, Baltimore, MD: Williams and Wilkins, pp. 17–19, 1982.
46. **Nakanishi N, Suzuki K, and Tatara K.** Clustered features of the metabolic syndrome and the risk for increased aortic pulse wave velocity in middle-aged Japanese men. *Angiology* 54: 551–559, 2003.
47. **Nashar K, Nguyen JP, Jesri A, Morrow JD, and Egan BM.** Angiotensin receptor blockade improves arterial distensibility and reduces exercise-induced pressor responses in obese hypertensive patients with the metabolic syndrome. *Am J Hypertens* 17: 477–482, 2004.
48. **North American Association for the Study of Obesity.** Statistical Summary Pages, http://www.naaso.org/statistics/, 2004.
49. **Renkin EM.** Control of microcirculation and blood-tissue exchange. *Handbook of Physiology*: *The Cardiovascular System*, Baltimore, MD: Williams and Wilkins, 1984, vol. IV, Part 2, pp. 627–689.
50. **Schwaninger RM, Sun H, and Mayhan WG.** Impaired nitric oxide synthase-dependent dilatation of cerebral arterioles in type II diabetic rats. *Life Sci* 73: 3415–3425, 2003.
51. **Scuteri A, Najjar SS, Muller DC, Andres R, Hougaku H, Metter EJ, and Lakatta EG.** Metabolic syndrome amplifies the age-associated increases in vascular thickness and stiffness. *J Am Coll Cardiol* 43: 1388–1395, 2004.
52. **Stainsby WN, B. Snyder B, and Welch, HG.** A pictographic essay on blood and tissue oxygen transport. *Med Sci Sports Exerc* 20: 213–221, 1998.
53. **Steinberg HO and Baron AD.** Vascular function, insulin resistance, and fatty acids. *Diabetologia* 45: 623–634, 2002.
54. **Stepp DW, Pollock DM, and Frisbee JC.** Low-flow vascular remodeling in the metabolic syndrome X. *Am J Physiol Heart Circ Physiol* 286: H964–H970, 2004.
55. **Stepp DW and Frisbee JC.** Augmented adrenergic vasoconstriction in hypertensive diabetic obese Zucker rats. *Am J Physiol Heart Circ Physiol* 282: H816–H820, 2002.
56. **Stuhlinger MC, Abbasi F, Chu JW, Lamendola C, McLaughlin TL, Cooke JP, Reaven GM, and Tsao PS.** Relationship between insulin resistance and an endogenous nitric oxide synthase inhibitor. *JAMA* 287: 1420–1426, 2002.
57. **Takiuchi S, Fujii H, Kamide K, Horio T, Nakatani S, Hiuge A, Rakugi H, Ogihara T, and Kawano Y.** Plasma asymmetric dimethylarginine and coronary and peripheral endothelial dysfunction in hypertensive patients. *Am J Hypertens* 17: 802–808, 2004.
58. **Tarpey MM and Fridovich I.** Methods of detection of vascular reactive species: nitric oxide, superoxide, hydrogen peroxide, and peroxynitrite. *Circ Res* 89: 224–236, 2001.
59. **Wiernsperger NF and Bouskela E.** Microcirculation in insulin resistance and diabetes: more than just a complication. *Diabetes Metab* 29: 6S77–6S87, 2003.
60. **Zhu J, Mori T, Huang T, and Lombard JH.** Effect of high-salt diet on NO release and superoxide production in rat aorta. *Am J Physiol Heart Circ Physiol* 286: H575–H583, 2004.